Growth of carbon fibres, sheets and tubes on diamond films under high power plasma etching conditions

I. Villalpando*, P. John and J.I.B. Wilson

School of Engineering and Physical Sciences, Heriot-Watt University,
Riccarton, Edinburgh, EH14 4AS, UK.
*Present address: Centro de Investigación de los Recursos Naturales, Antigua Normal Rural,
Salaices, López, Chihuahua, México.
e-mail: isaelav@hotmail.com

The application of diamond as a plasma facing material for fusion reactors can be limited by unknown reactions between diamond and the chamber materials transported by the plasma. Transformation of diamond to other structures can cause problems such as contamination of the plasma with loose particles or retention of gases. We have seen that diamond thin films are eroded under hydrogen plasma etching, but if silicon is present the growth of various carbon structures on diamond films is observed. We have produced carbon with different morphologies on diamond films including fibres, sheets with flower-like shapes and tubes and proposed growth mechanisms based on the results of Scanning Electron Microscopy, X-Ray Photoelectron Spectroscopy and Raman Spectroscopy.

Sample surfaces contain silicon and are oxidised having COO and CO groups as seen by XPS analysis. Raman analyses revealed a spectrum typical for graphite combined with that from diamond that remains on the surface after hydrogen bombardment. The results of this study show the experimental conditions in which carbon fibres, sheets and tubes are produced under high-power hydrogen etching of diamond films and open the possibility to other applications such as catalysts, sensors and the production of electrodes.

Keywords: Diamond; carbon fibres; carbon sheets; chemical vapour deposition; scanning electron microscopy.

PACS: 81.05.U; 81.05.ug; 81.05.uf

1. Introduction

Diamond films have been proposed for protecting plasma-facing components in tokamak fusion reactors [1]. In common with other materials such as graphite, contamination of the plasma and chamber with hydrocarbons and particulates is of concern. Whilst it is known that hydrogen bombardment etches carbon films there is little information about the surface transformation to other carbon structures that may worsen contamination leading to the retention of radioactive isotopes within fusion reactors. In the case of diamond, both theoretical [2] and related experimental studies [3-5] have shown that, under particle bombardment, the diamond lattice is converted to a high density thin amorphous carbon layer rather than graphite.

Under chemical vapour deposition (CVD) conditions various carbon structures have been reported, *e.g.* diamond (nano and poly-crystalline) [6], nanotubes and nanofibres [7], nanospheres [8], nanopipes [9], and micro-trees [10], among others. Experimental conditions to grow different structures vary in temperature (500 to 900°C) [11], pressure (30 to 760 torr), carbon source (methane, acetylene, benzene, ethylene being the most common) [12-15], and DC bias (150-400 V) [16]. We know that fibres as well as nanotubes and other nanostructures [17] are synthesised in catalytic CVD using catalyst particles such as Fe, Ni, Co, Cu or their alloys. Metal thin films have also been used as catalysts: the technique allows the formation of metal nanoparticles after thermal or plasma etching of the film [12,18].

Carbon structures have been produced for applications such as: energy storage [14], catalyst support materials [19-21], composite materials [22], selective adsorption agents [23,24], electrodes [25-27] and the production of flat panel displays, nano-transistors in computer technology [28-31], among others.

The aim of this work is to study the formation of fibres, sheets and tubes on diamond film substrates during hydrogen etching conditions in the presence of silicon. The diamond films used in this study exhibited different characteristics such as morphology and diamond quality (sp^3/sp^2 ratio) and the resulting fibres, sheets and tubes growth mechanisms are related to the substrate and hydrogen etching conditions.

2. Experimental

The nanocrystalline diamond films materials, exhibiting different morphology and sp^3/sp^2 ratio, were deposited by different growth conditions selected from previously reported experiments [32]. Diamond film deposition and fibre production were carried out in a 2.45 GHz microwave plasma enhanced CVD reactor described elsewhere [33]. The reactor design, for the growth of electronic grade diamond, eliminated the need for a quartz bell jar or other source of silicon near the plasma. Graphite substrates for diamond deposition were 20×20×3 mm^3 highly oriented pyrolytic graphite (HOPG) pieces (Ringsdorff Werke GmbH, Bonn, Germany).

Diamond film deposition was achieved under the following conditions. For sample 1, the film was grown on an ultra-
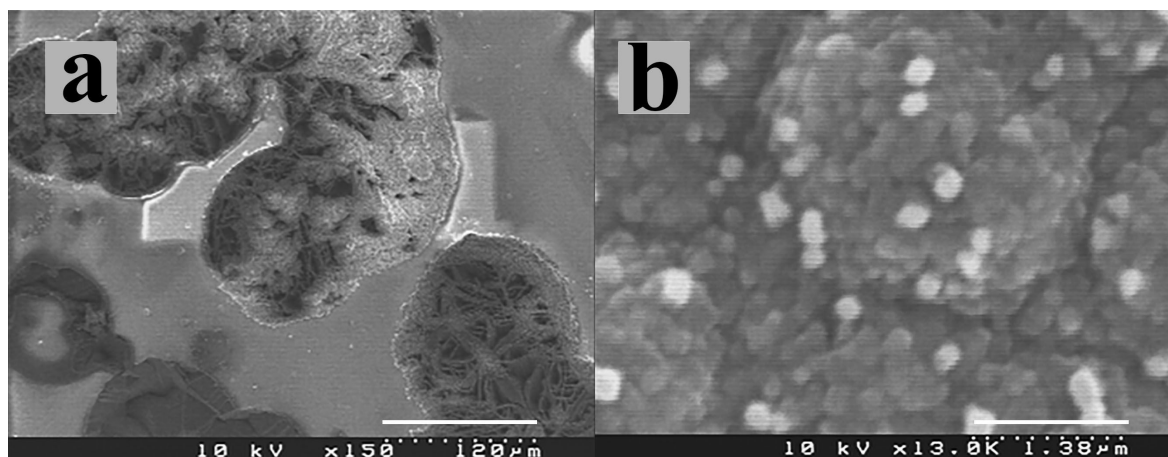
FIGURE 1. SEM micrographs from (a) etched silicon piece on the top of diamond films during fibre growth, (b) cumuli formation in nanodiamond films.

sonically scratched substrate (Bandelin Sonorex Digital 10P ultrasonic bath, for 30 min) with a suspension of 3% nanodiamond/methanol (detonation nanodiamond was cleaned by the procedure described by Jiang and Xu [34]) and CVD deposition was carried out using 1.5 kW input microwave power. Sample 2 was treated as sample 1 but CVD deposition was achieved using 3 kW input microwave power. For sample 3 the film was prepared on an ultrasonically scratched substrate with 3% microdiamond in methanol (1 μm natural diamond, de Beers) and CVD deposition was carried out using 3 kW input microwave power. For Sample 4, the film was grown on an untreated substrate using 1.5 kW input microwave power.

The gas mixture used in all the experiments was 5% CH_4/15% H_2/80% Ar with a total gas pressure of 100$\pm$2 torr, for 2 hours. For the growth of carbon fibres, sheets and tubes a crystalline silicon (5$\times$5 mm^2) wafer was placed on top of the pre-deposited diamond and a hydrogen plasma treatment was carried out for 15 min using 4.2 kW power at 50 $\pm$ 2 torr. All substrates were heated by the plasma, without additional heating, and the sample temperature was measured using a two-colour optical pyrometer.

Samples were characterised by scanning electron microscopy (SEM, Hitachi 2700, operated at 10 keV electron energy and with a secondary electron emission detector). Sample 2 was also analysed by SEM at the Electron Microscope Facility, University of St. Andrews, UK (Jeol JSM 5600, operated at 5 keV). Raman spectroscopy (Renishaw Ltd, inVia Raman microscope) used an excitation wavelength of 514.5 nm. The Raman spectra were collected from 1000 to 2000 cm^{-1} and the data were fitted using Gaussian profiles in OriginLab$^{\copyright}$ Data Analysis. X-Ray Photoelectron Spectroscopy (XPS) measurements, using Mg Kα X-radiation, were carried out in a Scienta ESCA300 spectrometer at the National Centre for Electron Spectroscopy and Surface Analysis (NCESS) UK. Deconvolution of the XPS peak profiles was performed using XPSPeak41 software using linear background correction and fitted to Lorentzian-Gaussian functions. The XPS peak positions were traceable to Au standard.

3. Results and Discussion

Hydrogen etching of diamond, under similar experimental conditions to those presented here, reveals steps and pits and removes primarily non-diamond carbonaceous material [35]. When a piece of silicon wafer is introduced on top of the samples, the silicon is etched (Fig. 1a) and the growth of fibres, sheets and tubes is seen in the vicinity. Carbon fibres, sheets and tubes were evident on the diamond substrate when silicon was present, through silicon transportation-inducing nucleation sites as observed in nanodiamond films (Fig. 1b).

Fibres grown on diamond films with different sp^3/sp^2 ratios (determined by deconvolution of the Raman spectra, Table I) present distinct morphologies. Lower quality diamond films (sp^3/sp^2 ratio) were etched faster, increasing the carbon (primarily in the form of methane) concentration in the plasma, which in turn will influence the ultimate carbon structures.

Sample 1 corresponds to thin bent fibres grown on a nanodiamond surface with sp^3/sp^2= 0.006 (Fig. 2a), with an approximate diameter of 360 nm (dimensions estimated by SEM micrographs) as shown in Fig. 2c. A high density of fibres was seen covering the film surface in this sample (Fig. 2b) compared to sample 2, evidently caused by a higher nucleation density. Since the etching of non-diamond material is more facile, a lower film quality will produce a higher carbon level above the surface resulting in a greater nucleation density. Fibres in Sample 2, were grown on a nanodiamond surface with a sp^3/sp^2 ratio of 0.017 (Fig. 3a). In contrast the resulting fibres were thicker and short (0.5 μm diameter and 3.5-4.5 μm length) with round tips resembling pins. There is a low fibre density on the diamond surface, indicating that nucleation was low (Fig. 3b). Fibres closer to the film surface were thinner but become thicker along the length of the fibre. The growth mechanism of the fibres in this case may be similar to that proposed by Bower *et al*. [36] for nanotubes. The growth of the fibres is from the bottom and
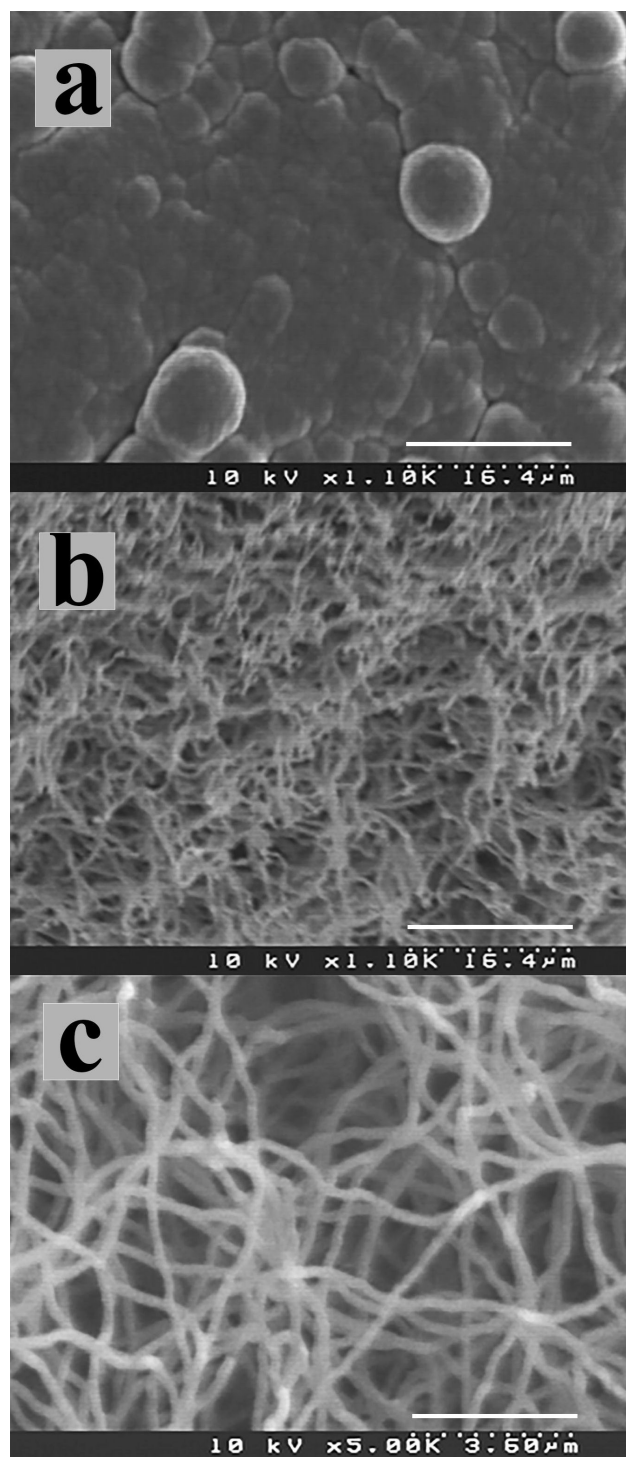
FIGURE 2. SEM micrographs from sample 1 showing: (a) nanocrystalline diamond film before carbon fibre growth; (b) fibre growth on diamond film, (c) bent and thin carbon fibres.
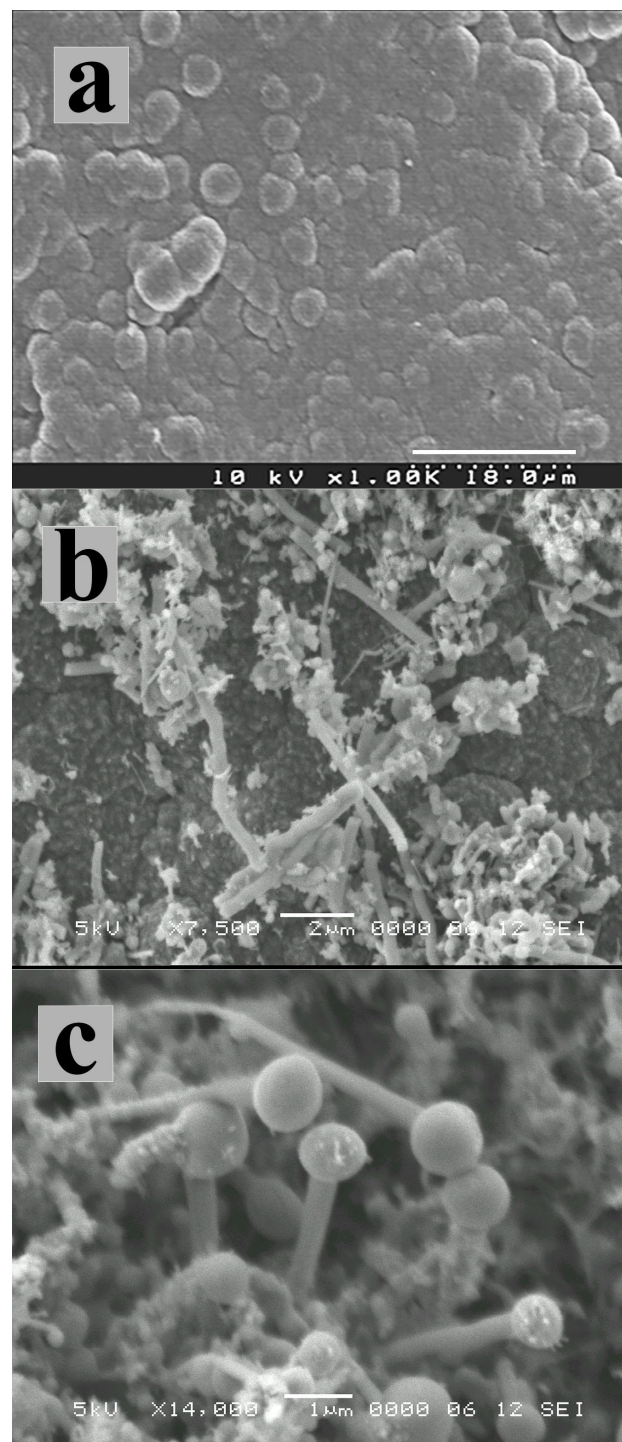

FIGURE 3. SEM micrographs from sample 2 showing: (a) nanocrystalline film, (b) after hydrogen etching showing fibre growth, (c) short and thick fibres with round tips resembling pins.

stops when the metal particle (catalyst) is saturated by carbon species; from that point the fibres begin to increase in diameter.

Wunderlich [16] proposed that low concentrations of carbon growing species produce thin nanotubes (*e.g.* single wall carbon nanotubes) that have fast reaction velocity. Multi-wall carbon nanotubes and graphite nanofibres have lower reaction velocities since they have to fill the three-dimensional volume. These features of the mechanism explain the variation of the thickness of fibres seen in samples 1 and 2. Thick and short fibres in sample 2 are the result of low reaction velocities, compared to the thin and long fibres in sample 1.
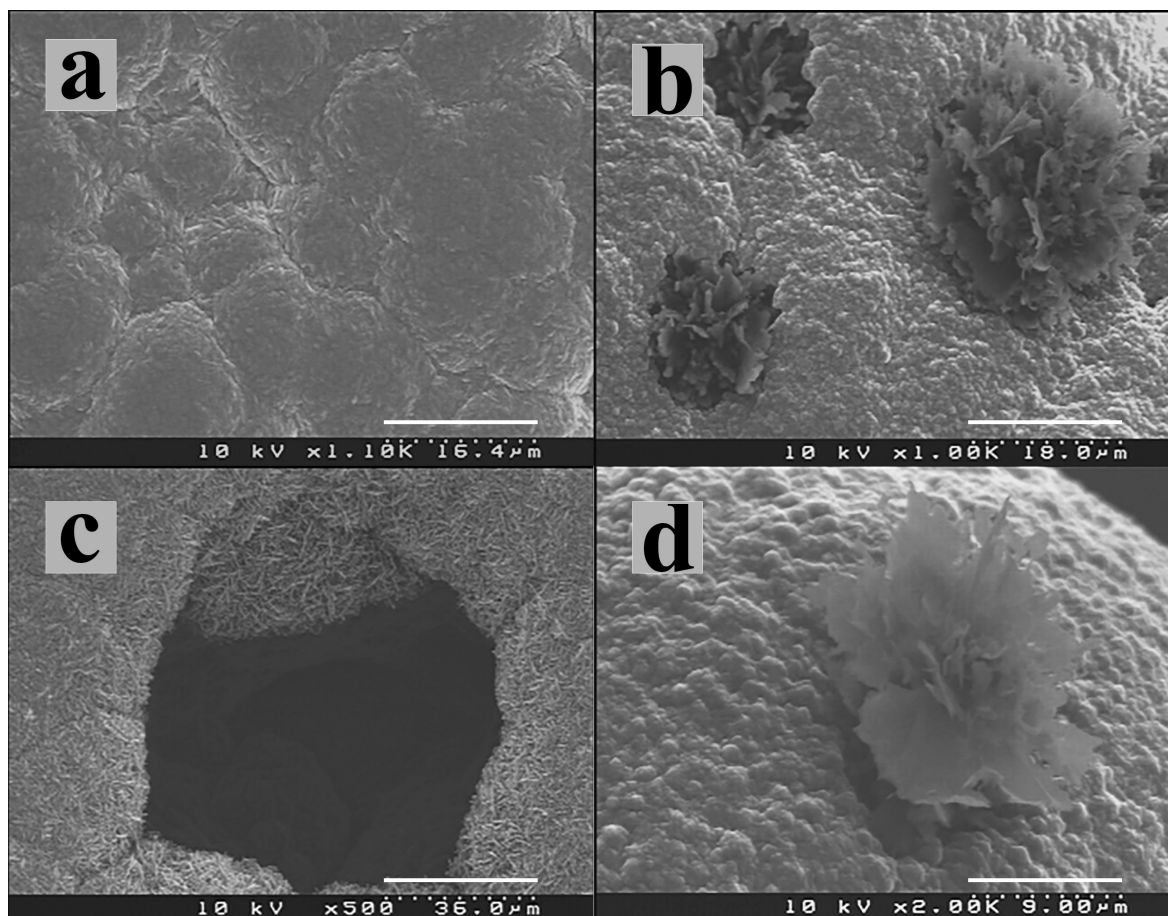
FIGURE 4. SEM micrographs from sample 3 showing: (a) nanocrystalline diamond film before carbon sheets growth; (b) sheets growth on diamond film, (c) etched pits showing initial growth of rod-like diamond. d) Single flower-like structure.

Sample 3 had sheets producing flower-like shapes (Fig. 4) that grow perpendicular to the diamond film in etched pits (Fig. 4b). Figure 4c shows an etched pit where the removed diamond surface reveals the first stage of diamond growth with rod-like morphology. We believe that carbon sheets grow onto the edges of these rods, and the different orientations of these rods produce the flower-like shape. The diamond quality is higher than samples 1, 2 and 4 and thus the etching rate and nucleation density is much lower. Similar flower-like shapes have been produced by laser ablation [37] and they have been synthesised in solvents under heating-cooling sequences [38,39] but to the best of our knowledge, this is the first time these structures have been observed under CVD conditions.

Figure 5 shows SEM micrographs from sample 4. For the nanocrystalline film shown in Fig. 5a, amorphous carbon growth (Fig. 5b) is evident after hydrogen treatment together with tubes of 600 nm in diameter and 750 nm length (Fig. 5c). It has been reported that the destruction of carbon nanotubes by bombardment occurs, forming conical shaped amorphous carbon layers, similar to the ones presented here [16]. We believe that the high etching rate of the film, and rapid deposition of graphitic material produce these amorphous materials.

In Fig. 6 we can see the results from the Raman spectroscopy analysis for all the samples. The spectra present contributions from nanocrystalline diamond or transpolyacetylene at 1135 and 1477 cm^{-1}; this feature has been attributed to the presence of polymeric sp^2 species at the grain boundaries [40]. The broad D-band at $\sim$1350 cm^{-1} and the G-band at $\sim$1550-1590 cm^{-1} are due to graphite. Samples 1, 2 and 3 also show the diamond peak at around 1332 cm^{-1} that arises from the substrate. The Raman analyses of the samples have contributions that correspond to the reported Raman spectra for graphite that exhibit two Raman-active modes. The E$_{2g}$ mode at around 1350 cm^{-1} has been related to polycrystalline graphite and its intensity depends on the particle size [41]. The second mode is the A$_{1g}$ at around 1580 cm^{-1} that has been identified with the doubly degenerate deformation mode of the hexagonal ring structure, observed in graphite single crystals. The signals from diamond suggest that each spectrum comprises contributions from the carbon fibres, sheets and tubes and the underlying diamond film.

The XPS spectra of nanocrystalline and polycrystalline layers (an example is presented in Fig. 7, from sample 1) show an intense and sharp C1s signal at a binding energy of $\sim$284.4 eV, with typical features characterised by the dia-

FIGURE 6. Raman spectra of the prepared samples containing carbon fibres, sheets and tubes grown on nanodiamond films substrates.

FIGURE 7. Typical deconvolution of C1s peak of the prepared carbon fibres, the one shown here corresponds to sample 1.
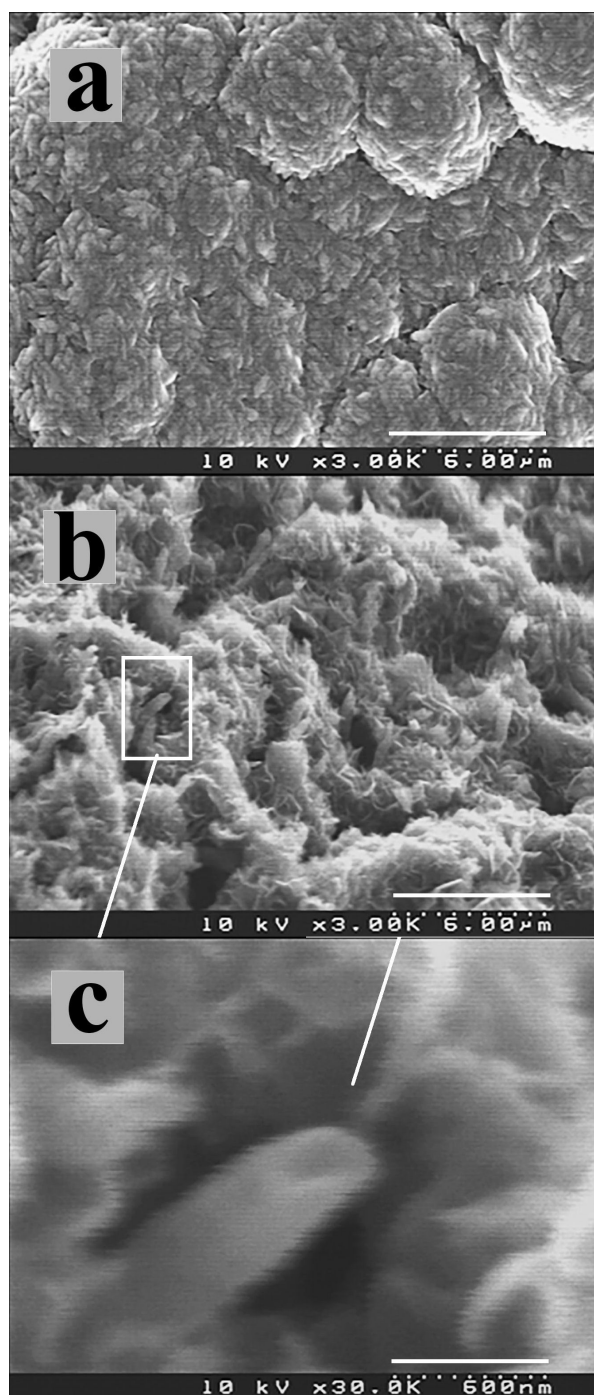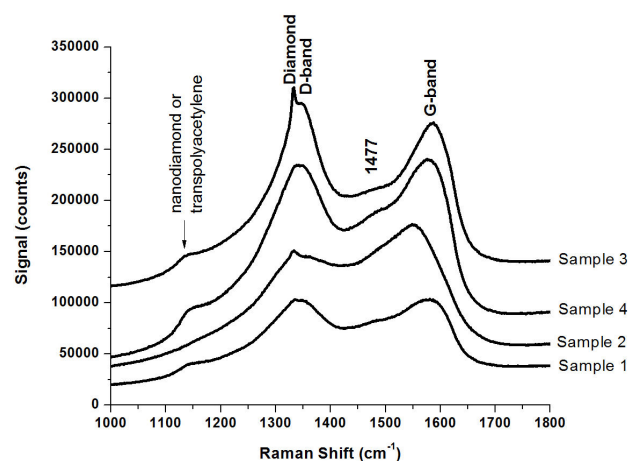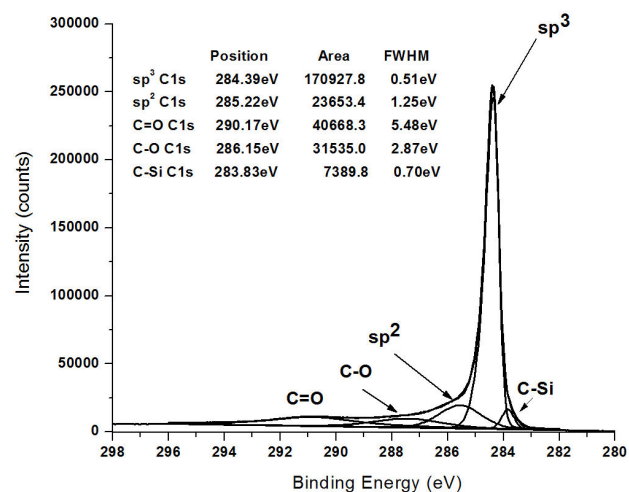
FIGURE 5. SEM micrographs from sample 4 showing: (a) nanocrystalline diamond film before carbon sheets growth; (b) amorphous carbon with some visible tubes; c) detail of tube.

mond structure [42,43]; the sp^2 carbon peak appears at ~285 eV and carbon bonded with oxygen (COH, COC, COOH, COOR) at ~286 and ~290 eV (see Fig. 7) [44]. Additionally, a silicon carbide (SiC) shoulder peak is at ~283.8 eV and is evidence for silicon being transported to the fibre tips during growth, especially in sample 1. The SEM analysis of sample 2 shows that silicon is covered by carbon material (similar to sample 4), thus diminishing the intensity

of the SiC signal. Sample 3 shows a low density of flower-like structures resulting in the XPS spectra being dominated by the diamond film. In all cases the carbon sp^3 peak is the highest intensity component (Table I).

XPS analysis of a pristine graphite substrate showed the presence of 1.2 at% of oxygen (not shown here) which, after diamond deposition, reduces to around 1 at% for all samples. After hydrogen etching, the oxygen content increased in samples 1, 2 and 3 to 26.33 at%, 17.90 at% and 6.40 at% respectively. The presence of peaks from ether and especially carboxylic acid (or ester) functional groups at ~288 eV, can be compared with carbon fibres that have been oxidised in strong acid mixtures [45]. Since oxygen is not deliberately added to the gas mixture it is probable that the samples were oxidised by exposure to air after removal from the CVD chamber.

TABLE I. sp^3/sp^2 ratio determined by Raman and XPS analyses of the sample surfaces from the areas of the core line spectra (% atomic).

Sample	sp^3/sp^2 ratio determined by Raman Spectroscopy	Carbon (sp^3C1s) determined by XPS (% atomic)	Carbon (sp^2C1s) determined by XPS (% atomic)	C-O bonds (O1s) determined by XPS (% atomic)	Silicon (2p) determined by XPS (% atomic)
1	0.006±0.001	62.35±6.2	8.61±0.9	26.33±2.6	2.69±0.3
2	0.017±0.002	57.58±5.8	23.18±2.3	17.90±1.8	1.33±0.1
3	0.042±0.003	67.87±6.8	22.25±2.2	0.99±0.1	8.88±0.9
4	——	85.58±8.6	5.17±0.5	6.40±0.6	2.84±0.3

4. Conclusions

The production of carbon fibres, sheets and tubes reported in this study provides information on the behaviour of diamond films under hydrogen plasma etching conditions in the presence of silicon. The carbon morphology of the fibres, sheets and tubes depended on the crystalline quality and structure of the diamond film used as a substrate. Silicon plays a key role in fibre production following plasma induce transportation to the fibres during growth. Flower-like shaped carbon structures were also observed following hydrogen plasma etching under different nucleation and plasma conditions than those used in the production of fibre or tubes. The surfaces of the structures were oxygen terminated as, evidenced by the XPS data.

The results of this work open the possibility to other applications such as catalysis, sensors and the production of electrodes, since they combine the unmatchable properties of a diamond supporting substrate with the unique properties of carbon fibres, sheets and tubes. These structures also offer some insight into the variety of formations that may arise from carbon that is hydrogen-plasma etched in the presence of additional elements, such as occurs in tokamak fusion reactor chemistry.

1. A.M. Stoneham, J.R. Matthews, and I.J. Ford, *J. Phys. Condens. Matter.* **16** (2004) S2597.

2. A.R. Dunn, and D.M. Duffy, *J. Appl. Phys.* **110** (2011) 104307.

3. S. Porro, G. De Temmerman, P. John, S. Lisgo, I. Villalpando, and J.I.B. Wilson, *Phys. Stat. Sol. (a)* **206** (2009) 2028.

4. G. De Temmerman *et al.*, *Phys. Scripta.* **T138** (2009) 014013.

5. S. Porro *et al.*, *Diam. Relat. Mater.* **19** (2010) 818.

6. P.K. Bachmann. In: *Popovici P.G, Bigelow L.K*, eds. Handbook of Industrial Diamonds and Diamond Films. (M.A., Marcel Dekker, INC, 1997)

7. A.V. Melechko *et al.*, *J. Appl. Phys.* **97** (2005) 041301.

8. J.Y. Miao *et al.*, *Carbon* **42** (2004) 813.

9. M. Kruk, M. Jaroniec, T.W. Kim, and R. Ryoo, *Chem. Mater.* **15** (2003) 2815.

10. P.M. Ajayan, J.M. Nugent, R.W. Siegel, B. Wei, and Ph. Kohler-Redlich, *Nature.* **404** (2000) 243.

11. B.O. Boskovic, V. Stolojan, R.U.A. Khan, S. Haq, and S.R.P. Silva, *Nat. Mater* **1** (2002) 165.

12. R.T.K. Baker, *Carbon* **27** (1989) 315.

13. M. Endo *et al.*, *J. Phys. Chem. Solids.* **54** (1993) 1841.

14. A. Chambers, C. Park, R. Terry, R.T.K. Baker, and N.M. Rodriguez, *J. Phys. Chem. B* **102** (1998) 4253.

15. A. Oberlin, M. Endo, and T. Koyama, *J. Cryst. Growth* **32** (1976) 335.

16. W. Wunderlich, *Diam. Relat. Mater.* **16** (2007) 369.

17. S. Porro *et al.*, *J. Non-Cryst. Solids.* **352** (2006) 1310.

18. N.M. Rodriguez, A. Chambers, R. Terry, and R.T.K. Baker, *Langmuir.* **11** (1995) 3862.

19. J.H. Bitter, M.K. Van der Lee, A.G.T. Slotboom, A.J. Van Dillen, and K.P. de Jong, *Catal. Lett.* **1-2** (2003) 139.

20. F. Rodriguez-Reinoso, *Carbon* **36** (1998) 159.

21. E. Boellaard, P.K. de Bokx, A.J.H.M. Kock, J.W. Geus. *J. Catal.* **96** (1985) 481.

22. G.G. Tibbetts, M.L. Lake, K.L. Strong, and B.P. Rice, *Compos. Sci. Technol.* **67** (2007) 1709.

23. G.A. Kovalenko *et al.*, Carbon, **39** (2001) 1033.

24. H. Suda, and K. Haraya, *J. Phys. Chem. B* **101** (1997) 3988.

25. B.T. Hang et al., *J. Power Sources.* **143** (2005) 256.

26. C.A. Bessel, K. Laubernds, N.M. Rodriguez, R.K.T. Baker, *J. Phys. Chem. B* **105** (2001) 1115.

27. S. Flandrois, and B. Simon, *Carbon.* **37** (1999) 165.

28. S. Fan *et al.*, *Science* **283** (1999) 512.

29. W. Hoenlein *et al.*, *Mater. Sci. Eng. C* **23** (2003) 663.

30. C. Bower, *Appl. Phys. Lett.* **77** (2000) 830.

31. R.H. Baughman, A.A. Zakhidov, and W.A. de Heer, *Science* **297** (2002) 787.

32. I. Villalpando, *Ph.D. Thesis.* (Heriot-Watt University, UK, 2010).

33. J.R. Rabeau, P. John, J.I.B. Wilson, and Y. Fan, *J. Appl Phys* **96** (2004) 6724.

34. T. Jiang, K. Wu, *Carbon.* **33** (1995) 1663.

35. I. Villalpando, P. John, S. Porro, and J.I.B. Wilson, *Diam. Relat. Mater.* **20** (2011) 711.

36. C. Bower, O. Zhou, W. Zhu, D.J. Werder, and S. Jin, *Appl. Phys. Lett.* **77** (2000) 2767.

37. V. Thongpool, P. Asanithia, and P. Limsuwan, *Procedia Eng.* **32** (2012) 1054.

38. T. Nakanishi *et al.*, *Small* (2007) 2019.

39. T. Nakanishi, *J. Phys Conf Ser* **159** (2009) 012005.

40. A.C. Ferrari, and J. Robertson, *Phys. Rev. B* **63** (2001) 121405.

41. S.N. Chaudhuri, R.A. Chaudhuri, R.E. Benner, and M.S. Penugonda, *Comp Struct*, **76** (2006) 375.

42. A. Cook, A.G. Fitzgerald, A.G. Storey, J.I.B. Wilson, P. John, and M.G. Jubber, *Diam. Relat. Mater.* **1** (1992) 478.

43. J.I.B. Wilson, J.S. Walton, and G. Beamson, *J. Elec. Spec. Rel. Phenom.* **121** (2001) 183.

44. G. Beamson, and D. Briggs, in *High Resolution XPS of Organic Polymers*: the Scienta ESCA300 Database, (Wiley, New York, 1992).

45. S.D. Gardner, C.S.K. Singamsetty, G.L. Booth, G.R. He, and C.U. Pittman, *Carbon*, **33** (1995) 587.